Journal of Applied Mathematics and Computing (2026) 72:63
https://doi.org/10.1007/s12190-025-02739-y

ORIGINAL RESEARCH

# On the stability of a finite difference scheme for the nonlinear silicon problem

**Adriano Rodrigues de Melo**[1,4] · **Marcio Augusto Villela Pinto**[2] · **Sebastião Romero Franco**[3,4] · **Priscila Dombrovski Zen**[4]

Received: 14 July 2025 / Revised: 10 November 2025 / Accepted: 1 December 2025


## Abstract

This paper introduces a finite difference numeric scheme designed for the computational solution of the nonlinear heat conduction problem in a homogeneous silicon rod. It is shown that the numerical method is consistent with the conservation law, is conditionally stable and convergent. Focusing on the implicit schemes, an efficient Newton multigrid method with Gauss-Seidel red-black smoother is developed. Computational experiments confirm the stability theory as well as the robustness of the multigrid method.

**Keywords** TVD stability · Nonlinear heat equation · Semiconductor · $\theta$ method

**MSC Classification** 65M12 · 65M55

✉ Adriano Rodrigues de Melo
adriano.melo@ifc.edu.br

Marcio Augusto Villela Pinto
marcio_villela@ufpr.br

Sebastião Romero Franco
romero@unicentro.br

Priscila Dombrovski Zen
prisciladzen@gmail.com

[1] Catarinense Federal Institute, BR-280, Araquari, Santa Catarina 89245-000, Brazil

[2] Department of Mechanical Engineering, Federal University of Paraná, Polytechnic Center, Curitiba, Paraná 81530-000, Brazil

[3] Department of Mathematics, State University of the Central West, Irati, Paraná 84505-677, Brazil

[4] Graduate Program in Numerical Methods in Engineering, Federal University of Paraná, Polytechnic Center, Curitiba, Paraná 81530-000, Brazil

Published online: 03 January 2026

## 1 Introduction

Nonlinear heat equations describe a significant diversity of processes, including the numerical modeling of gas filtration in porous media [1], the description of the phenomenon of thermal oxidation of silicon [2, 3], the study of heat transfer in human tissue [4], the problem of observer design, important in the microchip manufacturing process in the semiconductor industry [5], the analysis of composite materials used in the modern aerospace and nuclear industries [6], among others.

In this work, we address the following nonlinear heat equation for modeling thermal conduction in a homogeneous silicon rod [7–9]:

$$\rho c_p \frac{\partial u}{\partial t} = \frac{\partial}{\partial x}\left(\kappa(u)\frac{\partial u}{\partial x}\right), \quad x \in (a,b), \quad t > 0, \tag{1}$$

where the variable $u(x,t)$ represents the temperature at position $x$ at an instant $t$, while $\rho$ refers to the density and $c_p$ to the heat capacity at constant pressure, which are assumed constant in the present model.

Thermal conductivity $\kappa$ often depends on temperature [10, 11], and in semiconductor materials it usually assumes an exponential form [12, 13]:

$$\kappa(u) = \kappa_0 e^{\chi u}, \tag{2}$$

where $\kappa_0$ is the value of its thermal conductivity at a reference temperature and $\chi$ is the temperature dependence coefficient associated with $\kappa$. This work adopts Dirichlet boundary conditions and, together with the initial conditions, complete the physical model. They are represented by:

$$u(x,0) = u_0(x), \quad x \in [a,b], \quad u(a,t) = u_a(t) \quad \text{and} \quad u(b,t) = u_b(t), \quad t > 0. \tag{3}$$

Existence and uniqueness results for this model were demonstrated by Rincon, Límaco and Liu [14].

In nonlinear diffusive problems, Dirichlet boundary conditions are fundamental. Hristov [15], analyzing models of fluid penetration in wood capillaries, showed that the relaxing Dirichlet boundary condition is physically more appropriate, considering that real wood impregnation processes occur in infinite baths. In the computational approach to modeling the glaciation of sea offshore pipelines completely exposed to seawater, Krivovichev [16] uses a mathematical model based on the Dirichlet problem for the nonlinear heat equation in the domain with fixed boundaries.

Computer simulations using thermal numerical models play a crucial role in improving technologies that are beneficial to several areas of science and engineering [17–19]. These computational models are primarily required to be accurate and stable. Classical central discretization schemes have higher accuracy, but can generate unphysical or spurious numerical fluctuations that generally reduce the quality of the numerical solution to an unusable level [19–21]. This numerical phenomenon, common in computational fluid dynamics (CFD), was revealed by VonNeumann and Richtmyer [22].

The analysis of finite difference schemes for nonlinear heat equations has been the subject of study by several researchers. Katayama et al. [23] demonstrated sufficient conditions for the stability of an explicit Euler scheme. From an empirical perspective, Filipov et al. [8] reported evidence of robustness and stability in first-order temporal discretizations using the implicit Euler method. Experiments with second-order discretizations by the Crank-Nicolson (CN) method, on the other hand, can demonstrate strong unphysical oscillations, as pointed out by Jooma and Harley [24].

In this work, we establish sufficient conditions for the stability of a family of explicit and implicit numerical schemes ($\theta$ method), designed for the computational solution of the nonlinear heat conduction model described by Eqs. (1)-(3), used, in particular, for semiconductor materials such as silicon. The focus, however, is on the implicit formulation, which will be addressed in an integrated manner with the multigrid method [25–28].

The rest of this paper is organized as follows. In Sect. 2 we present the development of the numerical model, followed by the consistency and stability properties. In Sect. 3 we describe the multigrid algorithm to accelerate convergence. In Sect. 4, we conduct numerical experiments designed to evaluate the schemes in terms of stability, accuracy and robustness. In Sect. 5, we discuss the main findings.

## 2 Numerical scheme and stability analysis

In this section, we present the development of the numerical model and some properties. Since $\chi = 0$ is the linear case, we can reformulate by rewriting the right-hand side of Eq. (1) as $(\kappa(u)u_x)_x = (\kappa(u))_{xx}/\chi$, for $\chi \neq 0$, so that this equation then becomes:

$$\rho c_p \frac{\partial u}{\partial t} = \frac{1}{\chi}\frac{\partial^2 \kappa(u)}{\partial x^2}, \quad \chi \neq 0, \quad x \in (a,b), \quad t > 0. \tag{4}$$

The numerical model will be developed from a spatial mesh of the form:

$$\Omega^h = \{x_i \in [a,b];\ x_i = a + (i-1)h,\ 1 \leq i \leq n_x\},$$

where $n_x$ is the number of points in the discretization and $h = (b-a)/(n_x - 1)$ is the spatial increment. We similarly define a temporal mesh as $t_n = n\tau \in [0,\ t_f]$, with $0 \leq n \leq n_t$, where $\tau = t_f/n_t$ is the time step, $t_f$ is the final time of the analysis and $n_t$ is the number of time steps.

We conduct the discretization of Eq. (4) by applying the finite difference method (FDM) using the central difference scheme (CDS) in the spatial direction, as well as the $\theta$ method [29] for the temporal approximation, with $\theta \in [0,1]$:

$$\frac{\rho c_p}{\tau}\left(u_i^n - u_i^{n-1}\right) = \theta f_i(\mathbf{u}^n) + (1-\theta) f_i(\mathbf{u}^{n-1}), \quad 1 < i < n_x, \quad 1 \leq n \leq n_t, \tag{5}$$

where $u_i^n = u(x_i, t_n)$, $\mathbf{u}^n = \left(u_1^n, \cdots, u_i^n, \cdots, u_{n_x}^n\right)$ and

$$f_i(\mathbf{u}^n) = \frac{\kappa_{i+1}^n - 2\kappa_i^n + \kappa_{i-1}^n}{\chi h^2}, \quad \kappa_i^n = \kappa(u_i^n), \quad 1 < i < n_x. \tag{6}$$

Equation (5) defines a family of explicit (if $\theta = 0$) and implicit (if $0 < \theta \leq 1$) numerical schemes for the computational solution of the partial differential equation (PDE) (4). In particular, for $\theta = 0$ we have an explicit Euler discretization, $\theta = 1$ we have an implicit Euler discretization, while for $\theta = 1/2$, a CN discretization.

### 2.1 Consistency

This section is dedicated to the study of consistency and has as its main result the following Theorem:

**Theorem 1** *The scheme defined by Eq. (5) approximates the PDE (4) with discretization error*

$$\begin{aligned}\mathcal{E}(h,\tau,\theta) = &-\frac{\rho c_p(2\theta-1)\tau}{2}\frac{\partial^2 u}{\partial t^2}(x_i,t_n)\\ &-\rho c_p\sum_{l=3}^{\infty}\tau^{l-1}\frac{\partial^l u}{\partial t^l}(x_i,t_n)\frac{(-1)^{l-1}}{l!}\left[(1-\theta)l-1\right]\\ &-\frac{2}{\chi}\sum_{l=2}^{\infty}\frac{h^{2(l-1)}}{(2l)!}\left[\theta\frac{\partial^{2l}\kappa}{\partial x^{2l}}(x_i,t_n)+(1-\theta)\frac{\partial^{2l}\kappa}{\partial x^{2l}}(x_i,t_{n-1})\right].\end{aligned} \tag{7}$$

***Proof*** Consider the following finite difference formulas:

$$\begin{aligned}\frac{\partial u}{\partial t}(x_i,t_n) &= \frac{u_i^n - u_i^{n-1}}{\tau} + \sum_{l=2}^{\infty}(-1)^l\frac{\tau^{l-1}}{l!}\frac{\partial^l u}{\partial t^l}(x_i,t_n),\\ \frac{\partial u}{\partial t}(x_i,t_{n-1}) &= \frac{u_i^n - u_i^{n-1}}{\tau} - \sum_{l=2}^{\infty}\frac{\tau^{l-1}}{l!}\frac{\partial^l u}{\partial t^l}(x_i,t_{n-1}),\\ \frac{\partial^2\kappa}{\partial x^2}(x_i,t_n) &= \frac{\kappa_{i+1}^n - 2\kappa_i^n + \kappa_{i-1}^n}{h^2} - 2\sum_{l=2}^{\infty}\frac{h^{2(l-1)}}{(2l)!}\frac{\partial^{2l}\kappa}{\partial x^{2l}}(x_i,t_n),\\ \frac{\partial^2\kappa}{\partial x^2}(x_i,t_{n-1}) &= \frac{\kappa_{i+1}^{n-1} - 2\kappa_i^{n-1} + \kappa_{i-1}^{n-1}}{h^2} - 2\sum_{l=2}^{\infty}\frac{h^{2(l-1)}}{(2l)!}\frac{\partial^{2l}\kappa}{\partial x^{2l}}(x_i,t_{n-1}).\end{aligned}$$

Substituting the expressions appropriately in Eq. (4) evaluated at the points $(x_i, t_n)$ and $(x_i, t_{n-1})$, we obtain, respectively:

$$\begin{aligned}\frac{\rho c_p}{\tau}\left(u_i^n - u_i^{n-1}\right) + \rho c_p\sum_{l=2}^{\infty}(-1)^l\frac{\tau^{l-1}}{l!}\frac{\partial^l u}{\partial t^l}(x_i,t_n) = \frac{\kappa_{i+1}^n - 2\kappa_i^n + \kappa_{i-1}^n}{\chi h^2} -\\ \frac{2}{\chi}\sum_{l=2}^{\infty}\frac{h^{2(l-1)}}{(2l)!}\frac{\partial^{2l}\kappa}{\partial x^{2l}}(x_i,t_n),\end{aligned} \tag{8}$$

$$\frac{\rho c_p}{\tau}\left(u_i^n - u_i^{n-1}\right) - \rho c_p \sum_{l=2}^{\infty} \frac{\tau^{l-1}}{l!}\frac{\partial^l u}{\partial t^l}(x_i, t_{n-1}) = \frac{\kappa_{i+1}^{n-1} - 2\kappa_i^{n-1} + \kappa_{i-1}^{n-1}}{\chi h^2} - \frac{2}{\chi}\sum_{l=2}^{\infty}\frac{h^{2(l-1)}}{(2l)!}\frac{\partial^{2l}\kappa}{\partial x^{2l}}(x_i, t_{n-1}). \tag{9}$$

Adding Eqs. (8) and (9) multiplied by $\theta$ and $1-\theta$ respectively, we obtain:

$$\begin{aligned}
&\frac{\rho c_p}{\tau}\left(u_i^n - u_i^{n-1}\right) = \theta f_i(\mathbf{u}^n) + (1-\theta) f_i(\mathbf{u}^{n-1}) \\
&- \rho c_p \sum_{l=2}^{\infty}\left\{\theta(-1)^l \frac{\partial^l u}{\partial t^l}(x_i, t_n) - (1-\theta)\frac{\partial^l u}{\partial t^l}(x_i, t_{n-1})\right\}\frac{\tau^{l-1}}{l!} \\
&- \frac{2}{\chi}\sum_{l=2}^{\infty}\left\{\theta\frac{\partial^{2l}\kappa}{\partial x^{2l}}(x_i, t_n) + (1-\theta)\frac{\partial^{2l}\kappa}{\partial x^{2l}}(x_i, t_{n-1})\right\}\frac{h^{2(l-1)}}{(2l)!}.
\end{aligned} \tag{10}$$

We use the Taylor series

$$\frac{\partial^l u}{\partial t^l}(x_i, t_{n-1}) = \frac{\partial^l u}{\partial t^l}(x_i, t_n) + \sum_{k=1}^{\infty}(-1)^k \frac{\tau^k}{k!}\frac{\partial^{l+k} u}{\partial t^{l+k}}(x_i, t_n), \quad l \geq 1,$$

to simplify the discretization error shown in Eq. (10), writing it as:

$$\begin{aligned}
\mathcal{E}(h, \tau, \theta) &= -\rho c_p \sum_{l=2}^{\infty}\frac{\tau^{l-1}}{l!}\left[\theta - 1 + \theta(-1)^l\right]\frac{\partial^l u}{\partial t^l}(x_i, t_n) \\
&+ (1-\theta)\rho c_p \sum_{l=2}^{\infty}\frac{\tau^{l-1}}{l!}\sum_{k=1}^{\infty}(-1)^k\frac{\tau^k}{k!}\frac{\partial^{l+k} u}{\partial t^{l+k}}(x_i, t_n) \\
&- \frac{2}{\chi}\sum_{l=2}^{\infty}\left\{\theta\frac{\partial^{2l}\kappa}{\partial x^{2l}}(x_i, t_n) + (1-\theta)\frac{\partial^{2l}\kappa}{\partial x^{2l}}(x_i, t_{n-1})\right\}\frac{h^{2(l-1)}}{(2l)!}.
\end{aligned} \tag{11}$$

By developing the double summation of the right-hand side of Eq. (11), we find:

$$\begin{aligned}
\sum_{l=2}^{\infty}\frac{\tau^{l-1}}{l!}\sum_{k=1}^{\infty}(-1)^k\frac{\tau^k}{k!}\frac{\partial^{l+k} u}{\partial t^{l+k}} &= \frac{\tau^1}{2!}\left\{(-1)^1\frac{\tau^1}{1!}\frac{\partial^3 u}{\partial t^3} + (-1)^2\frac{\tau^2}{2!}\frac{\partial^4 u}{\partial t^4} + (-1)^3\frac{\tau^3}{3!}\frac{\partial^5 u}{\partial t^5} + \right. \\
&\left. (-1)^4\frac{\tau^4}{4!}\frac{\partial^6 u}{\partial t^6} + \cdots\right\} + \frac{\tau^2}{3!}\left\{(-1)^1\frac{\tau^1}{1!}\frac{\partial^4 u}{\partial t^4} + (-1)^2\frac{\tau^2}{2!}\frac{\partial^5 u}{\partial t^5} + \right. \\
&\left. (-1)^3\frac{\tau^3}{3!}\frac{\partial^6 u}{\partial t^6} + (-1)^4\frac{\tau^4}{4!}\frac{\partial^7 u}{\partial t^7} + \cdots\right\} + \frac{\tau^3}{4!}\left\{(-1)^1\frac{\tau^1}{1!}\frac{\partial^5 u}{\partial t^5} + \right. \\
&\left. (-1)^2\frac{\tau^2}{2!}\frac{\partial^6 u}{\partial t^6} + (-1)^3\frac{\tau^3}{3!}\frac{\partial^7 u}{\partial t^7} + (-1)^4\frac{\tau^4}{4!}\frac{\partial^8 u}{\partial t^8} + \cdots\right\} + \cdots
\end{aligned}$$

Next, we group similar terms together:

$$\begin{aligned}
&\sum_{l=2}^{\infty}\frac{\tau^{l-1}}{l!}\sum_{k=1}^{\infty}(-1)^k\frac{\tau^k}{k!}\frac{\partial^{l+k}u}{\partial t^{l+k}} = (-1)^1\frac{\tau^2}{2!1!}\frac{\partial^3 u}{\partial t^3}\\
&+\left[\frac{(-1)^2}{2!2!}+\frac{(-1)^1}{3!1!}\right]\tau^3\frac{\partial^4 u}{\partial t^4}\\
&+\left[\frac{(-1)^3}{2!3!}+\frac{(-1)^2}{3!2!}+\frac{(-1)^1}{4!1!}\right]\tau^4\frac{\partial^5 u}{\partial t^5}+\cdots,\\
&=\sum_{l=3}^{\infty}\sum_{k=1}^{l-2}\frac{(-1)^k}{k!(l-k)!}\tau^{l-1}\frac{\partial^l u}{\partial t^l}.
\end{aligned} \tag{12}$$

Substituting Eq. (12) into Eq. (11) and organizing the sums, we find:

$$\begin{aligned}
\mathcal{E}(h,\tau,\theta) &= -\frac{\rho c_p(2\theta-1)\tau}{2}\frac{\partial^2 u}{\partial t^2}(x_i,t_n)\\
&-\rho c_p\sum_{l=3}^{\infty}\tau^{l-1}\frac{\partial^l u}{\partial t^l}(x_i,t_n)\left\{\frac{\theta(-1)^l+\theta-1}{l!}-(1-\theta)\sum_{k=1}^{l-2}\frac{(-1)^k}{k!(l-k)!}\right\}\\
&-\frac{2}{\chi}\sum_{l=2}^{\infty}\frac{h^{2(l-1)}}{(2l)!}\left\{\theta\frac{\partial^{2l}\kappa}{\partial x^{2l}}(x_i,t_n)+(1-\theta)\frac{\partial^{2l}\kappa}{\partial x^{2l}}(x_i,t_{n-1})\right\}.
\end{aligned} \tag{13}$$

From the Binomial Theorem [29], for $l \geq 3$, we have:

$$(1-1)^l=\sum_{k=0}^{l}\frac{l!}{k!(l-k)!}1^{n-k}(-1)^k=\frac{l!(-1)^0}{0!l!}+\sum_{k=1}^{l-2}\frac{l!(-1)^k}{k!(l-k)!}+\frac{l!(-1)^{l-1}}{(l-1)!1!}+\frac{l!(-1)^l}{l!0!},$$

that is,

$$\sum_{k=1}^{l-2}\frac{l!(-1)^k}{k!(l-k)!}=-1-l(-1)^{l-1}-(-1)^l,\quad l\geq 3.$$

With this, we can simplify the term that appears in Eq. (13):

$$\frac{\theta(-1)^l+\theta-1}{l!}-(1-\theta)\sum_{k=1}^{l-2}\frac{(-1)^k}{k!(l-k)!}=S_l(\theta),$$

where

$$S_l(\theta)=\frac{\theta(-1)^l+\theta-1}{l!}-(1-\theta)\left[\frac{-1-l(-1)^{l-1}-(-1)^l}{l!}\right]=\frac{(-1)^{l-1}}{l!}\left[(1-\theta)l-1\right]. \tag{14}$$

□

Finally, substituting Eq. (14) into Eq. (13), we obtain Eq. (7) for the discretization error.

Provided that one chooses $\theta$ such that $\theta \to c$ when $\tau \to 0$, for some constant $c \in \mathbb{R}$, Theorem 1 shows that $\mathcal{E}(h, \tau, \theta) \to 0$ when $h, \tau \to 0$ and so the scheme is consistent. In particular, this holds for $\theta$ fixed within the interval $[0, 1]$.

It is clear that for $\theta = 1/2$ (CN), the asymptotic order of the discretization error is 2, while for fixed values of $\theta \in [0, 1] \setminus \{1/2\}$, the asymptotic order becomes 1. A more general strategy for achieving second-order accuracy is presented below:

**Corollary 1.1** *Let $c \in \mathbb{R}$. If $\theta \in [0, 1]$ is such that $2\theta - 1 = \tau\theta'$, for some fixed $\theta'$ or with $\theta' \to c$ when $\tau \to 0$, and $-1 \leq \tau\theta' \leq 1$, then scheme (5) is consistent and the asymptotic order of the discretization error is $\mathcal{O}(\tau^2, h^2)$.*

***Proof*** Indeed, the definition $2\theta - 1 = \tau\theta'$ implies that $\theta \to 1/2$ when $\tau \to 0$ and the scheme is consistent. Furthermore, $0 \leq \theta \leq 1$ implies that $-1 \leq 2\theta - 1 \leq 1$. Finally, the discretization error becomes:

$$\begin{aligned} \mathcal{E}(h, \tau, \theta) &= -\frac{\rho c_p \theta' \tau^2}{2} \frac{\partial^2 u}{\partial t^2}(x_i, t_n) + \mathcal{O}(\tau^2) + \mathcal{O}(h^2), \\ &= \mathcal{O}(\tau^2, h^2). \end{aligned}$$

□

In this work, another form of consistency is considered: the one that relates the flux functions of the conservation law and the discrete model [30]. Thus, to proceed, note that the scheme given in Eq. (5) can be rewritten in conservative form as:

$$u_i^n = u_i^{n-1} - \frac{\tau}{h}\left[F\left(u_i^n, u_{i+1}^n, u_i^{n-1}, u_{i+1}^{n-1}\right) - F\left(u_{i-1}^n, u_i^n, u_{i-1}^{n-1}, u_i^{n-1}\right)\right], \quad (15)$$

where

$$\begin{aligned} F\left(u_i^n, u_{i+1}^n, u_i^{n-1}, u_{i+1}^{n-1}\right) = &-\frac{\theta}{\rho c_p \chi h}\left[\kappa\left(u_{i+1}^n\right) - \kappa\left(u_i^n\right)\right] \\ &- \frac{(1-\theta)}{\rho c_p \chi h}\left[\kappa\left(u_{i+1}^{n-1}\right) - \kappa\left(u_i^{n-1}\right)\right], \end{aligned} \quad (16)$$

denotes the numerical flux.

A method written as in Eq. (15) is consistent with the underlying conservation law if its numerical flux reduces to the true flux in the case of constant flow [20, 30–32]. Thus, let $u(x, t) \equiv \bar{u}$ be constant, since the true flux of Eq. (4) is $-(\rho c_p \chi)^{-1} \partial\kappa(u)/\partial x$, we conclude by analyzing Eq. (16) that:

$$F(\bar{u},\bar{u},\bar{u},\bar{u}) = 0 = -\frac{1}{\rho c_p \chi}\frac{\partial \kappa(\bar{u})}{\partial x}.$$

Furthermore, since $F$ is continuous and differentiable on every open $V \in \mathbb{R}^4$, it follows that $F$ is Lipschitz continuous on every bounded open set $V$. Thus, scheme (15), and therefore (5), is consistent with conservation law (4).

### 2.2 Stability

In this section we will use the concept of total variation (TV) stability, defined according to LeVeque [30] as follows:

**Definition 1** [30] A numerical method is total variation stable, or simply TV-stable, if all the approximations for $\tau < \tau_0$ lie in some fixed set of the form

$$\mathcal{K} = \{u \in L_{1,T} : \ TV_T(u) \leq R \quad \text{and} \quad supp\,(u(\cdot,t)) \subset [-M,M] \quad \forall\, t \in [0,T]\}\,, \tag{17}$$

where $R > 0$ and $M > 0$ may depend on the initial data and the flux function, but not on $\tau$.
In Definition 1, $supp(u(\cdot,t))$ represents the support of the function $u(\cdot,t)$ and $supp(u(\cdot,t)) \subset [-M,M]$ means that $u(\cdot,t) \equiv 0$ for all $|x| > M$ (under these conditions, $u$ is said to have compact support). Furthermore, $L_{1,T}$ designates the space of functions consisting of all functions of $x$ and $t$ in which the norm $||\cdot||_{1,T}$ is finite and is computed as:

$$||v||_{1,T} = \int_0^T ||v(\cdot,t)||_1 dt = \int_0^T \int_{-\infty}^{\infty} |v(x,t)| dx dt.$$

Finally, the quantity TV translated to mesh functions is calculated as [30]:

$$TV_T(\mathbf{u}^n) = \sum_{n=0}^{T/\tau} \left[\tau TV(\mathbf{u}^n) + \left|\left|\mathbf{u}^{n+1} - \mathbf{u}^n\right|\right|_1\right] \quad \text{and} \quad TV(\mathbf{u}^n) = \sum_{i=-\infty}^{\infty} \left|u_{i+1}^n - u_i^n\right|.$$

In LeVeque [30] and in Harten [31] one can find the demonstration of the following convergence result concerning the TVs methods:

**Theorem 2** *[30] Suppose $\mathbf{u}^n$ is generated by a numerical method in conservation form with a Lipschitz continuous numerical flux, consistent with some scalar conservation law. If the method is TV-stable, then method converges to a weak solution.*

The consistency associated with the conservation law was discussed and verified in Sect. 2.1. Therefore, in order for Theorem 2 to be employed, TV stability must be proven.

To ensure the compactness required in Definition 1, we assume initial data with bounded total variation and with compact support on the contours. Furthermore, it

is assumed that the mesh functions are zero for all points outside the boundaries. To achieve the requirement of TV stability related to the existence of a constant $R > 0$, we will use the following concept:

**Definition 2** [31]. A numerical scheme is total variation diminishing stable (TVD-stable), when it is possible to obtain:

$$TV(\mathbf{u}^{n+1}) \leq TV(\mathbf{u}^n), \tag{18}$$

for all mesh functions $\mathbf{u}^n$ associated with the method.
It can be shown that, for initial data with bounded total variation, the inequality (18) implies the existence of $R > 0$, such that $TV_T(\mathbf{u}^n) \leq R$, so that Definition 1 is satisfied [30].

**Definition 3** [30]. A numerical method is $l_1$-contracting if, for any two grid functions $\mathbf{u}^{n-1}$ and $\mathbf{v}^{n-1}$ for which $\mathbf{u}^{n-1} - \mathbf{v}^{n-1}$ has compact support, the grid functions $\mathbf{u}^n$ and $\mathbf{v}^n$ satisfy

$$||\mathbf{u}^n - \mathbf{v}^n||_1 \leq ||\mathbf{u}^{n-1} - \mathbf{v}^{n-1}||_1.$$

Additionally, it can be shown that every $l_1$-contracting method is TVD and holds Eq. (18) [30]. In short, for a numerical method to be TVD-stable, it is sufficient that it be $l_1$-contracting. In this context, we present the main result of this section:

**Theorem 3** *Let $0 \leq \theta \leq 1$. If*

$$0 \leq (1-\theta)\frac{\tau}{h^2}\frac{\kappa(\beta)}{\rho c_p} \leq \frac{1}{2}, \quad \text{with} \quad \min_i \left\{u_i^{n-1}, v_i^{n-1}\right\} \leq \beta \leq \max_i \left\{u_i^{n-1}, v_i^{n-1}\right\}, \tag{19}$$

*whatever the mesh functions $\mathbf{u}^{n-1}$ and $\mathbf{v}^{n-1}$, then the numerical scheme in Eq. (5) is $l_1$-contracting.*

***Proof*** Let two mesh functions $\mathbf{u}^{n-1}$ and $\mathbf{v}^{n-1}$ be those in which $\mathbf{u}^{n-1} - \mathbf{v}^{n-1}$ has compact support, and consider the functions $\mathbf{u}^n$ and $\mathbf{v}^n$ generated by the numerical scheme (5). Then,

$$\begin{aligned} u_i^n - v_i^n =& u_i^{n-1} - v_i^{n-1} + \\ & \frac{\tau}{\rho c_p}\{\theta\left[f_i\left(\mathbf{u}^n\right) - f_i\left(\mathbf{v}^n\right)\right] + (1-\theta)\left[f_i\left(\mathbf{u}^{n-1}\right) - f_i\left(\mathbf{v}^{n-1}\right)\right]\}. \end{aligned} \tag{20}$$

From the mean value theorem, for some $\beta_i^n$ between $u_i^n$ and $v_i^n$, we write:

$$\kappa(u_i^n) - \kappa(v_i^n) = \chi\kappa(\beta_i^n)\left(u_i^n - v_i^n\right),$$

so we can simplify the term $f_i\left(\mathbf{u}^n\right) - f_i\left(\mathbf{v}^n\right)$, with $f_i$ defined according to Eq. (6), as follows:

$$f_i\left(\mathbf{u}^n\right) - f_i\left(\mathbf{v}^n\right) = \frac{\chi\kappa(\beta_{i+1}^n)\left(u_{i+1}^n - v_{i+1}^n\right) - 2\chi\kappa(\beta_i^n)\left(u_i^n - v_i^n\right) + \chi\kappa(\beta_{i-1}^n)\left(u_{i-1}^n - v_{i-1}^n\right)}{\chi h^2}.$$

Thus, after considering $w_i^n = u_i^n - v_i^n$, we can rewrite Eq. (20) as:

$$\begin{aligned} w_i^n &= w_i^{n-1} \\ &+ \frac{\tau}{\rho c_p h^2}\left\{\theta\left[\kappa(\beta_{i+1}^n)w_{i+1}^n - 2\kappa(\beta_i^n)w_i^n + \kappa(\beta_{i-1}^n)w_{i-1}^n\right] + \right. \\ &\left.(1-\theta)\left[\kappa(\beta_{i+1}^{n-1})w_{i+1}^{n-1} - 2\kappa(\beta_i^{n-1})w_i^{n-1} + \kappa(\beta_{i-1}^{n-1})w_{i-1}^{n-1}\right]\right\}, \end{aligned}$$

or even,

$$\begin{aligned} \left[1 + \frac{2\theta\tau}{\rho c_p h^2}\kappa\left(\beta_i^n\right)\right] w_i^n = \left[1 - \frac{2(1-\theta)\tau}{\rho c_p h^2}\kappa\left(\beta_i^{n-1}\right)\right] w_i^{n-1} + \frac{\theta\tau}{\rho c_p h^2}\left[\kappa(\beta_{i+1}^n)w_{i+1}^n + \right. \\ \left. \kappa(\beta_{i-1}^n)w_{i-1}^n\right] + \frac{(1-\theta)\tau}{\rho c_p h^2}\left[\kappa(\beta_{i+1}^{n-1})w_{i+1}^{n-1} + \kappa(\beta_{i-1}^{n-1})w_{i-1}^{n-1}\right]. \end{aligned} \tag{21}$$

With the auxiliary parameter

$$\alpha_i^n = \frac{\tau}{h^2}\frac{\kappa(\beta_i^n)}{\rho c_p},$$

we use Eq. (21) to establish the following inequality:

$$\begin{aligned} &|1 + 2\theta\alpha_i^n|\,|w_i^n| \le \left|1 - 2(1-\theta)\alpha_i^{n-1}\right|\left|w_i^{n-1}\right| \\ &+ \theta\left|\alpha_{i+1}^n\right|\left|w_{i+1}^n\right| + \theta\left|\alpha_{i-1}^n\right|\left|w_{i-1}^n\right| \\ &+ |1-\theta|\left|\alpha_{i+1}^{n-1}\right|\left|w_{i+1}^{n-1}\right| + |1-\theta|\left|\alpha_{i-1}^{n-1}\right|\left|w_{i-1}^{n-1}\right|, \end{aligned}$$

which is used to form the following sums:

$$\begin{aligned} h\sum_{i=-\infty}^{\infty}|1 + 2\theta\alpha_i^n|\,|w_i^n| \le h\sum_{i=-\infty}^{\infty}\left|1 - 2(1-\theta)\alpha_i^{n-1}\right|\left|w_i^{n-1}\right| + \theta h\sum_{i=-\infty}^{\infty}\left|\alpha_{i+1}^n\right|\left|w_{i+1}^n\right| + \\ \theta h\sum_{i=-\infty}^{\infty}\left|\alpha_{i-1}^n\right|\left|w_{i-1}^n\right| + |1-\theta|h\sum_{i=-\infty}^{\infty}\left|\alpha_{i+1}^{n-1}\right|\left|w_{i+1}^{n-1}\right| + |1-\theta|h\sum_{i=-\infty}^{\infty}\left|\alpha_{i-1}^{n-1}\right|\left|w_{i-1}^{n-1}\right|. \end{aligned} \tag{22}$$

Then, using hypothesis (19), the fact that $0 \le \theta \le 1$ and $\alpha_i^n > 0$, we can combine the terms of the index of the summation, in order to obtain:

$$h\sum_{i=-\infty}^{\infty}\left[1+2\theta\alpha_i^n\right]\left|w_i^n\right| \le h\sum_{i=-\infty}^{\infty}\left[1-2(1-\theta)\alpha_i^{n-1}\right]\left|w_i^{n-1}\right| + \theta h\sum_{i=-\infty}^{\infty}\alpha_i^n\left|w_i^n\right| +$$
$$\theta h\sum_{i=-\infty}^{\infty}\alpha_i^n\left|w_i^n\right| + (1-\theta)h\sum_{i=-\infty}^{\infty}\alpha_i^{n-1}\left|w_i^{n-1}\right| + (1-\theta)h\sum_{i=-\infty}^{\infty}\alpha_i^{n-1}\left|w_i^{n-1}\right|.$$

Since the terms cancel, we finally conclude that:

$$||\mathbf{u}^n-\mathbf{v}^n||_1 = h\sum_{i=-\infty}^{\infty}\left|w_i^n\right| \le h\sum_{i=-\infty}^{\infty}\left|w_i^{n-1}\right| = ||\mathbf{u}^{n-1}-\mathbf{v}^{n-1}||_1,$$

and the scheme Eq. (5) is $l_1$-contracting.□

The convergence follows directly from the fact that scheme (5) is a weak contraction in the $l_1$ norm. Indeed, if $v(x,t)\in C^4\left([a,b]\times[0,t_f)\right)$ is a solution to Eq. (4) that satisfies condition (19), then $v$ satisfies the scheme (5) except for the discretization error, Eq. (7), as shown in Eq. (10). It follows from this that if $u_i^n$ is a solution produced by the numerical scheme for a certain set of initial data satisfied by $v$ and if $E_i^n = v(x_i,t_n)-u_i^n$, then an estimate for the error can be obtained by (following the proof of the mentioned Theorem):

$$||\mathbf{E}^n||_1 \le ||\mathbf{E}^{n-1}||_1 + \mathcal{O}\left(\tau,h^2\right), \quad 1\le n\le n_t,$$

implying that:

$$||\mathbf{E}^n||_1 \le ||\mathbf{E}^0||_1 + \mathcal{O}\left(\tau,h^2\right), \quad 1\le n\le n_t.$$

Theorem 2 establishes, however, that the differentiability assumption can be considerably relaxed since, being TVD-stable, it converges to a weak solution.

***Remark 1*** Analyzing the issue of well-posedness for an initial-boundary value problem (IBVP) defined by a more general one-dimensional PDE, Rincon, Límaco and Liu [14] adopted as their main assumption the boundedness of the functions $\kappa(u)$, $u_0(x)$ and their derivatives. Oleinik and Kruzhkov [33], in a previous work, also adopted this boundedness assumption on compact domains to establish the well-posedness of an even more general multidimensional problem. In this sense, the IBVP (1)-(3) satisfies these assumptions and is well-posed. Furthermore, an IBVP with Neumann boundary conditions was investigated by Gavrilut and Morosanu [34].

A direct consequence of Theorem 3 is the following Corollary:

**Corollary 3.1** *The implicit Euler method applied to Eq. (4) is unconditionally TVD-stable.*

***Proof*** It suffices to note that, when $\theta = 1$, constraint (19) holds, regardless of the mesh parameters.

Similar results were reported by Harten [31], Yee, Warming and Harten [20] and Yee [32].

### 2.3 Stability versus accuracy

The criterion established in Corollary 1.1, for schemes of order 2, consists of writing $\theta$ in such a way that we have $2\theta - 1 = \tau\theta'$, with $-1 \leq \tau\theta' \leq 1$. On the other hand, from the stability condition (19) imposed by Theorem 3, we obtain:

$$1 - \left(\frac{\tau}{h^2}\frac{\kappa(\beta)}{\rho c_p}\right)^{-1} \leq \tau\theta' \leq 1. \tag{23}$$

The inequality (23) indicates that any relation of the type $\tau = ch$, $c > 0$, degenerates the precision of the scheme to order 1, as the mesh is refined, since we have in this case:

$$1 - \frac{h}{c}\frac{\rho c_p}{\kappa(\beta)} \leq \tau\theta' \leq 1 \quad \Rightarrow \quad \tau\theta' \xrightarrow{h\to 0} 1 \quad \Rightarrow \quad \theta \xrightarrow{h\to 0} 1,$$

that is, the scheme tends to the implicit Euler method.

In the following section we discuss how to include the multigrid accelerator in solving the system of equations generated by the discretization.

## 3 Newton-MG solver

The multigrid method (MG) can be described as an iterative technique designed for the efficient solution of large-scale linear systems, obtained as discrete models for PDEs [25–28]. It uses a hierarchy of grids, where information flows through the restriction operator $I_h^H$, which transfers information from the fine grid $\Omega^h$ to the immediately coarser grid $\Omega^H$, and the prolongation operator $I_H^h$, which transfers information from the coarse grid $\Omega^H$ to the immediately finer grid $\Omega^h$. A commonly used way to generate the $\Omega^H$ grid is the standard coarsening strategy, which consists of doubling the $\Omega^h$ grid spacing in all directions [25]. In this case, we say that the coarsening ratio ($cr$) is 2, that is, $H = 2h$.

The desired numerical solution is calculated on the finer grid, while on the coarser grids, where the smoothers are more efficient [35], the correction estimates are calculated. The number of smoothings preceding the restriction and prolongation operators are denoted by $\nu_1$ (number of pre-smoothings) and $\nu_2$ (number of post-smoothings), respectively, while the manner in which the grids are visited is called a cycle. In this work, cycles of type $V$ will be used, also denoted by $V(\nu_1, \nu_2)$ [25, 36, 37].

Corrections can be made using two approaches: the correction scheme (CS), which uses only the residual in the correction process, and the full approximation scheme (FAS), which, in addition to the residual, also uses the approximate solution itself in its correction strategy [25, 36]. In the context of nonlinear problems, both

approaches can be used [38]. The CS strategy, however, must be preceded by a global linearization.

In this paper we use a Newton linearization in conjunction with the CS scheme. Algorithm 1 describes the CS scheme with cycles of type $V(\nu_1, \nu_2)$ and standard coarsening ratio ($cr = 2$), for the smoothing of the linear system at the grid level $l$. This algorithm implements the Gauss-Seidel red-black (GS-RB) smoother, which updates the even rows first and only then updates the odd rows.

**Algorithm 1** MG($l$).

**Require:** Input data, initial and boundary conditions

**while** Stopping criterion is not reached **do**
  **if** $l = L_{\max}$ **then**
    solve the system $\mathbf{A}^{lh}\mathbf{v}^{lh} = \mathbf{f}^{lh}$ on the coarse grid $\Omega^{2^l h}$
  **else**
    smooth $\nu_1$ times $\mathbf{A}^{lh}\mathbf{v}^{lh} = \mathbf{f}^{lh}$ on the grid $\Omega^{2^l h}$ with the GS-RB solver
    compute the defect $\mathbf{r}^{lh} = \mathbf{f}^{lh} - \mathbf{A}^{lh}\mathbf{v}^{lh}$ on the grid $\Omega^{2^l h}$
    restrict the defect $\mathbf{f}^{(l+1)h} = I_{2^l h}^{2^{l+1}h}\mathbf{r}^{lh}$ from grid $\Omega^{2^l h}$ to grid $\Omega^{2^{l+1}h}$
    solve at the next level: $\mathbf{MG}(l+1)$
    interpolate and correct the approximation: $\mathbf{v}^{lh} \leftarrow \mathbf{v}^{lh} + I_{2^{l+1}h}^{2^l h}\mathbf{v}^{(l+1)h}$
    smooth $\nu_2$ times $\mathbf{A}^{lh}\mathbf{v}^{lh} = \mathbf{f}^{lh}$ on the grid $\Omega^{2^l h}$ with the GS-RB solver
  **end if**
**end while**

Algorithm 2 incorporates the MG technique with the time-stepping (TS) sweep [39], so that at each time step $n$ a proper linear system is defined, via Newton's method, which is smoothed with Algorithm 1. Among the listed objects, $\mathbf{J}^{n,\nu-1}$ is the Jacobian matrix and $\mathbf{r}^{n,\nu-1}$ is the residual, both calculated from Eq. (5), using the approximation of iterate $\nu - 1$.

**Algorithm 2** TS-Newton-MG.

**Require:** Input data, initial and boundary conditions

**for** $n = 2 : n_t$ **do**
  initialize: $\nu$, $\mathbf{u}^{n,\nu-1}$, $\mathbf{r}^{n,\nu-1}$ and $\mathbf{J}^{n,\nu-1}$
  **while** Stopping criterion is not reached **do**
    set $\mathbf{A}^h = \mathbf{J}^{n,\nu-1}$, $\mathbf{v}^h = \mathbf{0}$, $\mathbf{f}^h = \mathbf{r}^{n,\nu-1}$
    solve the linear system $\mathbf{A}^h\mathbf{v}^h = \mathbf{f}^h$ using Algorithm 1: MG(1)
    update $\mathbf{u}^{n,\nu} \leftarrow \mathbf{u}^{n,\nu-1} + \mathbf{v}^h$
    compute $\mathbf{J}^{n,\nu}$ and $\mathbf{r}^{n,\nu}$
    update $\nu \leftarrow \nu + 1$
  **end while**
**end for**

## 4 Numerical experiments

In this section we discuss the computational experiments designed to evaluate the numerical schemes and the implemented code for solving the nonlinear heat transfer problem in a silicon rod. The purpose is also to confirm the theory detailed in this paper. We focus on the implicit Euler and CN methods, so when referring to the Euler method it should be clear that it is the implicit formulation.

The values of the physical parameters adopted in the experiments follow Filipov and Faragó [7], and consider a thin and homogeneous rod in the interval $x \in [1, 3]$, excluding heat or radiation sources, with constant Dirichlet boundary conditions: $u(1, t) = 2$ and $u(3, t) = 1$, $t > 0$. The following initial temperature profile is assumed:

$$u(x, 0) = 2 - \frac{x - 1}{2} + (x - 1)(x - 3), \quad x \in [1, 3].$$

The density and heat capacity associated with silicon were fixed at $\rho = 2.33$ and $c_p = 0.7$, respectively [40]. The parameters $\kappa_0$ and $\chi$, on the other hand, were varied. The final time was $t_f = 2$ s, during which the steady state was reached in most of the cases listed.

The source code was implemented in the Fortran language with the GNU Fortran compiler (GFortran), uses double precision and was executed on an operating system equipped with an Intel® Core™i5-7200 U processor, featuring a central processing unit (CPU) operating at 2.50 GHz and 16 GB of RAM.

The MG stopping criterion is the infinite norm of the dimensionless residual of the $k$-th iteration with respect to the initial estimate, according to a tolerance $\varepsilon_{MG}$:

$$\frac{||\mathbf{r}^k||_\infty}{||\mathbf{r}^0||_\infty} < \varepsilon_{MG} = 10^{-10}, \quad k \geq 1. \tag{24}$$

Regarding the stopping criterion associated with linearizations, an estimate of the relative error calculated in the infinite norm was used, taking the increment corresponding to consecutive linearizations divided by the current approximation, and subject to a tolerance $\varepsilon_{Lin}$:

$$\frac{||\mathbf{u}^{n,\nu} - \mathbf{u}^{n,\nu-1}||_\infty}{||\mathbf{u}^{n,\nu}||_\infty} < \varepsilon_{Lin} = 10^{-10}, \quad \nu \geq 1, \quad 2 \leq n \leq n_t. \tag{25}$$

Finally, the other MG settings were: cycles of type $V(1, 1)$, standard coarsening $(cr = 2)$, restriction operator $I_h^{2h}$ by full weighting and prolongation operator $I_{2h}^h$ by linear interpolation [25, 36, 37].

***Remark 2*** The one-dimensional case presented in this paper is intended for comparison with results in the literature, in particular with the work of Filipov and Faragó [7] and Zen et al. [9]. All the numerical tools used here can be extended to the two-dimensional case and are currently under development.

### 4.1 Formation of non-physical oscillations

In order to confirm the theory, we begin this section with simulations that employ a mesh configuration of the type $\tau = h$.

We vary the parameter $\theta$ (with increments of 0.05) and consider four settings for the pair $(\kappa_0, \chi)$, chosen to provide different smoothness patterns in the numerical solution. To compute $h$, we use $n_x = 2^{n_g} + 1$, where $n_g$ is the number of grid levels. In this experiment, we set $n_g = 5$. Table 1 contains the average number of linearization and MG cycles. For $\theta$ below 0.45, all cases considered either diverged or did not converge (in the limit of 50 linearizations/MG cycles).

For a qualitative perception, in Fig. 1 we consider the graphs of the numerical solutions calculated at the central point ($x = x_c$), for $\theta$ equal to 0.5 (CN), 0.75 and 1 (Euler). Euler's method is stable in all cases, as theory predicts. The mixed method ($\theta = 0.75$) starts to show oscillations in the last parameter configuration tested, while the CN method shows oscillation in two configurations.

Additionally, we observe that the CN method is more oscillatory the more intense the nonlinearity is (expressed by the magnitude of the parameters $\kappa_0$ and $\chi$). For example, the combination $\kappa_0 = 0.5$ and $\chi = 0.1$ indicates little intensity in the thermal conductivity $\kappa = \kappa_0 e^{\chi u}$, generating a smooth solution, and the CN method works well. In the combination $\kappa_0 = 100.0$ and $\chi = 2.0$, on the other hand, we observe an abrupt change in temperature in the initial milliseconds, causing strong instability. For a global perception about this oscillatory pattern, Fig. 2 shows the numerical solutions in the space/time domain computed by the CN and Euler methods.

In the next experiment, we modify the mesh parameter configuration to fulfill the condition of Theorem 3. Table 2 presents the data from this simulation. There was convergence in all cases. Furthermore, the average linearization number and the number of MG cycles were both relatively low.

In particular, in Fig. 3 we show the behavior of the Euler and CN solutions, computed at the central point $x_c$, adopting the equality $\tau/h^2 = \rho c_p/\kappa_{\max}$, where $\kappa_{\max} = \max\{\kappa(u_i^{n-1})\}$ and $h$ is calculated using $n_g = 5$. The temperature reaches

**Table 1** Average linearization number and number of MG cycles (in parentheses), calculated with $n_g = 5$ grids and different values of $\theta$, considering a mesh configuration $\tau = h$

| $\theta$ | $(\kappa_0, \chi)$ | | | |
|---|---|---|---|---|
| | (0.5, 0.1) | (1.0, 1.0) | (10.0, 1.0) | (100.0, 2.0) |
| $\leq 0.40$ | * | * | * | * |
| 0.45 | 4.8 (6.8) | * | * | * |
| 0.50 | 3.5 (8.0) | 4.0 (6.1) | 4.5 (3.9) | 7.2 (3.0) |
| 0.55 | 3.5 (8.9) | 3.3 (7.2) | 3.6 (3.8) | 3.7 (3.0) |
| 0.60 | 3.5 (8.9) | 3.1 (8.0) | 3.0 (3.7) | 2.8 (3.0) |
| 0.65 | 3.5 (8.9) | 3.1 (8.1) | 2.7 (3.6) | 2.2 (3.0) |
| 0.70 | 3.5 (8.9) | 3.1 (8.0) | 2.2 (3.5) | 1.9 (3.0) |
| 0.75 | 3.5 (8.9) | 3.1 (8.0) | 2.0 (3.5) | 1.8 (3.0) |
| 0.80 | 3.5 (8.8) | 3.2 (8.0) | 1.8 (3.4) | 1.6 (3.0) |
| 0.85 | 3.5 (8.7) | 3.2 (7.9) | 1.7 (3.3) | 1.5 (3.0) |
| 0.90 | 3.5 (8.7) | 3.2 (7.9) | 1.7 (4.2) | 1.5 (3.0) |
| 0.95 | 3.5 (8.6) | 3.2 (7.8) | 1.8 (4.1) | 1.4 (3.0) |
| 1.00 | 3.5 (8.6) | 3.2 (7.7) | 1.8 (4.2) | 1.3 (3.0) |

Note: The asterisk (*) indicates divergence or non-convergence

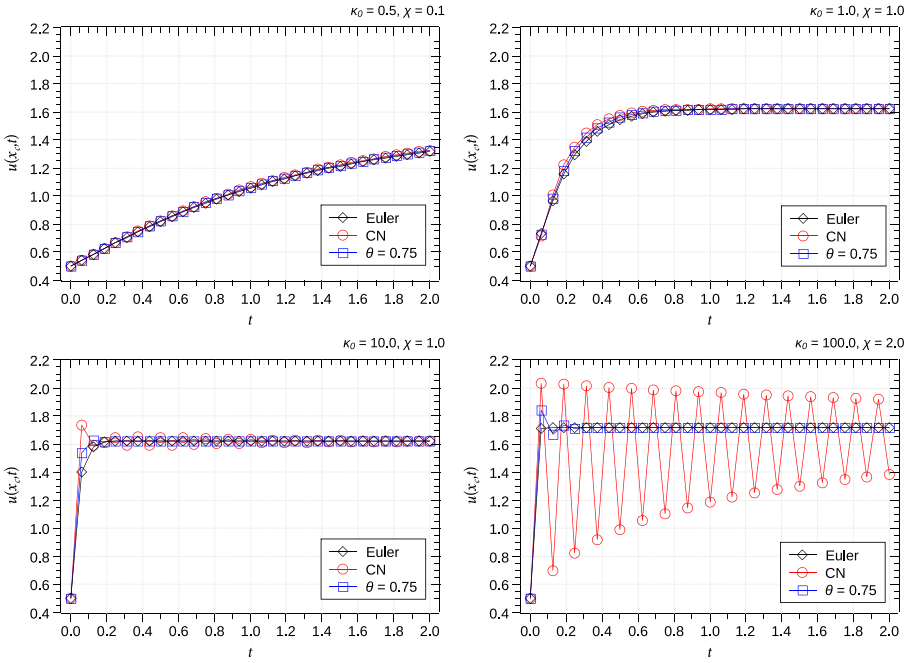


**Fig. 1** Numerical solutions by the CN, Euler and mixed methods ($\theta = 0.75$), computed in $x_c$, considering the degree of smoothness associated with the combinations between the parameters $\kappa_0$ and $\chi$

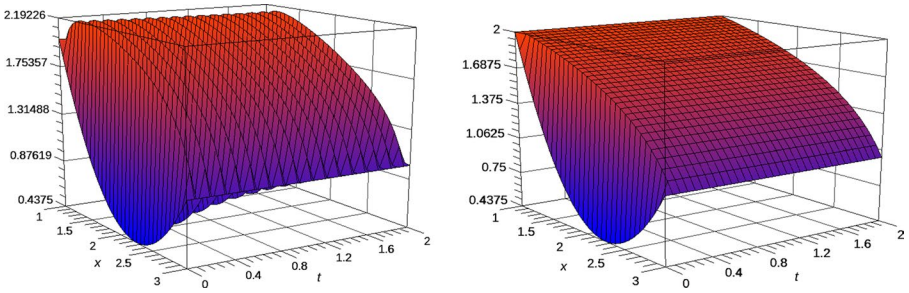


**Fig. 2** Numerical solutions by the CN (left) and Euler (right) methods for $\kappa_0 = 100.0$ and $\chi = 2.0$

steady state within the first few thousandths of a second. As expected by theory, we see that unphysical oscillations no longer occur.

## 4.2 Apparent order

For code verification, we use the concept of the apparent order $p_U$ of the discretization error of the numerical solution, indicated when the analytical solution is unknown [41]. This metric allows us to computationally verify whether the order of the numerical solution tends to the asymptotic order $p_L$ of the discretization error, as the mesh spacing $h$ is reduced. It can be calculated as follows [9]:

**Table 2** Average number of linearizations and number of MG cycles (in parentheses), calculated with $n_g = 5$ grids and different values of $\theta$, considering a stabilized mesh configuration

| $\theta$ | $(\kappa_0, \chi)$ | | | |
|---|---|---|---|---|
| | (0.5, 0.1) | (1.0, 1.0) | (10.0, 1.0) | (100.0, 2.0) |
| 0.05 | 2.2 (3.0) | 2.1 (3.0) | 1.1 (3.0) | 1.0 (5.0) |
| 0.10 | 2.3 (3.6) | 2.2 (3.8) | 1.1 (3.2) | 1.0 (5.0) |
| 0.15 | 2.4 (4.0) | 2.2 (4.0) | 1.1 (4.0) | 1.0 (5.0) |
| 0.20 | 2.4 (4.0) | 2.2 (4.0) | 1.1 (4.0) | 1.0 (5.0) |
| 0.25 | 2.4 (4.9) | 2.2 (5.0) | 1.1 (5.0) | 1.6 (4.9) |
| 0.30 | 2.5 (5.0) | 2.2 (5.0) | 1.1 (5.0) | 1.0 (5.0) |
| 0.35 | 2.5 (5.6) | 2.2 (5.8) | 1.1 (5.2) | 1.0 (5.0) |
| 0.40 | 2.5 (6.0) | 2.3 (6.0) | 1.1 (5.2) | 1.0 (5.0) |
| 0.45 | 2.5 (6.0) | 2.3 (6.0) | 1.1 (6.0) | 1.0 (6.0) |
| 0.50 | 2.6 (6.8) | 2.3 (6.9) | 1.2 (5.4) | 1.0 (5.0) |
| 0.55 | 2.6 (7.0) | 2.3 (7.0) | 1.7 (7.0) | 1.0 (5.0) |
| 0.60 | 2.6 (7.5) | 2.3 (7.8) | 1.2 (5.6) | 1.0 (5.0) |
| 0.65 | 2.6 (7.7) | 2.3 (7.9) | 1.2 (5.6) | 1.0 (5.0) |
| 0.70 | 2.7 (8.0) | 2.3 (8.0) | 1.2 (5.7) | 1.0 (5.0) |
| 0.75 | 2.7 (8.6) | 2.4 (8.8) | 1.2 (5.8) | 1.0 (5.0) |
| 0.80 | 2.8 (8.7) | 2.4 (8.8) | 1.2 (5.9) | 1.0 (5.0) |
| 0.85 | 2.8 (8.9) | 2.4 (9.0) | 1.2 (5.9) | 1.0 (5.0) |
| 0.90 | 3.0 (9.5) | 2.5 (9.8) | 1.2 (6.1) | 1.0 (5.0) |
| 0.95 | 3.2 (9.6) | 2.6 (9.8) | 1.2 (8.4) | 1.0 (5.0) |
| 1.00 | 3.6 (8.9) | 3.3 (8.0) | 1.9 (4.3) | 1.3 (3.0) |

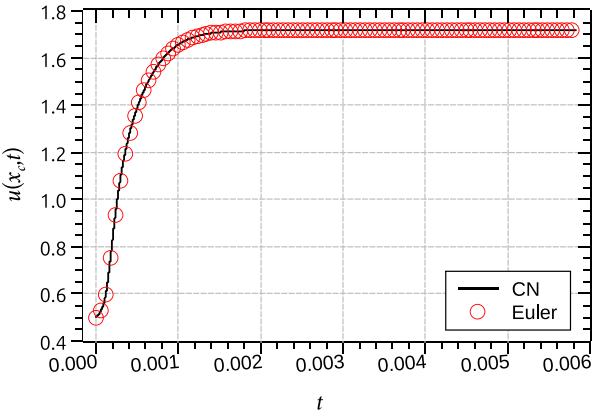


**Fig. 3** Numerical solution by the Euler and CN methods, evaluated at $x_c$, considering $\tau/h^2 = \rho c_p/\kappa_{\max}$ (CN stability condition), $\kappa_0 = 100.0$ and $\chi = 2.0$

$$p_U = \frac{\log\left|\dfrac{\phi_2 - \phi_3}{\phi_1 - \phi_2}\right|}{\log(q)}, \tag{26}$$

where $\phi_1$, $\phi_2$ and $\phi_3$ are the numerical solutions calculated in the fine, coarse and super-coarse meshes, with respective spacings $h_1$, $h_2$ and $h_3$, and refinement ratio $q = h_3/h_2 = h_2/h_1$.

In calculating $p_U$, we used $q = 2$, quadruple precision, and enough iterations for Eqs. (24) and (25) to reach rounding error. This approach seeks to isolate the effects of discretization error, in order to minimize other sources of error [9].

Figure 4 shows a graphical representation of the test implemented for two variables: average temperature ($u_m$) and temperature at the center of the domain ($u_c$), both calculated at the last time step, considering the case $\kappa_0 = 0.1$ and $\chi = 0.5$. As expected, as the mesh is refined, the apparent order $p_U$ tends towards the asymptotic orders $p_L = 1$ (Euler) or $p_L = 2$ (CN), depending on the method used.

After code verification, we proceed with the numerical results related to the MG method.

### 4.3 Average convergence factor

To evaluate the MG method, we use the average convergence factor $\rho_M$, a metric that represents the average reduction factor of the residual after one MG cycle [25, 37]. In this work, it is calculated from the arithmetic mean of the asymptotic convergence factor $\rho_m^k$ [42]:

$$\rho_M = \frac{1}{n_t}\sum_{j=1}^{n_t}\overline{\rho}_m^j, \quad \overline{\rho}_m^j = \frac{1}{it_{Lin}}\sum_{k=1}^{it_{Lin}}\rho_m^k, \quad \rho_m^k = \sqrt[it_{MG}]{\frac{||\mathrm{r}^{it_{MG}}||_\infty}{||\mathrm{r}^0||_\infty}}, \tag{27}$$

where $it_{MG}$ is the number of MG cycles of the $k$-th linearization, $it_{Lin}$ is the number of linearizations in the $j$-th time step and $n_t$ the total number of time steps.

Figures 5 and 6 show the evolution of the average convergence factor $\rho_M$ in terms of the number of unknowns $\mathbf{N} = n_t(n_x - 2)$, calculated for various combinations of the parameters $\kappa_0$ and $\chi$, for $\theta = 1$ (Euler) and $0.75$ (Fig. 5) and $\theta = 0.5$ (CN) and $0.25$ (Fig. 6).

MG methods are more efficient the closer to zero $\rho_M$ is and, conversely, the closer to unity the lower their efficiency [36]. We observe that $\rho_M$ stabilizes at values below $0.107$ (when $\theta = 1$) as the mesh is refined, regardless of the choice of physical parameters, indicating efficiency and robustness of the MG.

The MG method proved to be independent of the stability criterion set out in Theorem 3. Indeed, the average convergence factor $\rho_M$ of the CN method, in the same settings as the Euler method (with $\tau = h$), produces results similar to those in Fig. 5

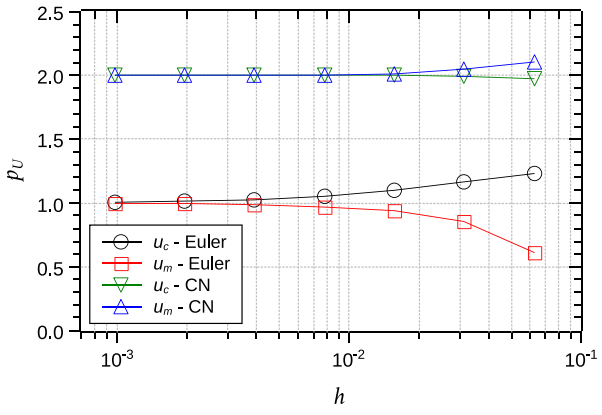


**Fig. 4** $p_U$ calculated for $u_c$ and $u_m$, at the final analysis time $t_f$, with the Euler and CN methods

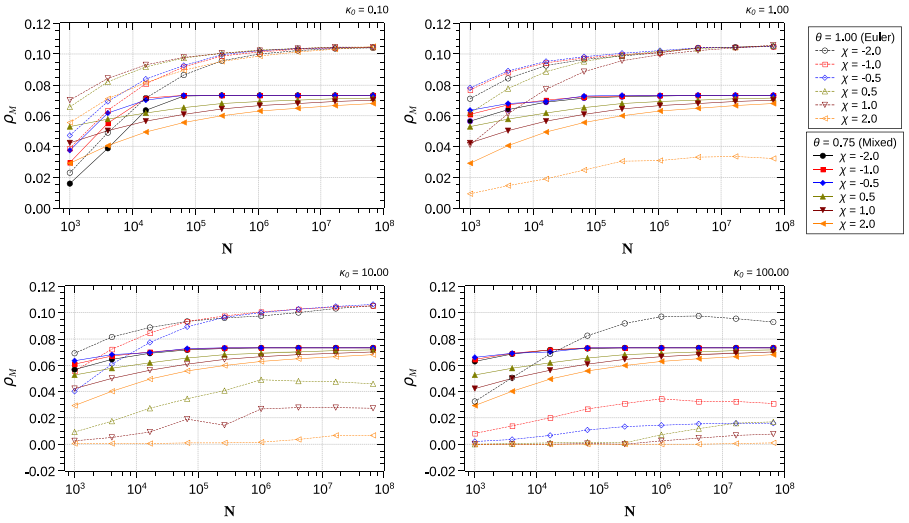


**Fig. 5** $\rho_M$ *versus* $\mathbf{N}$, calculated for the Euler and mixed ($\theta = 0.75$) method, with different combinations of parameters

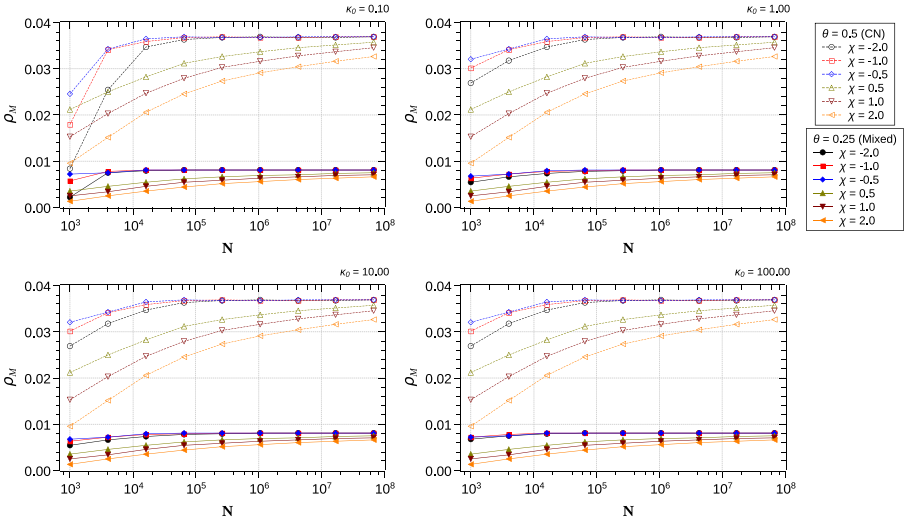


**Fig. 6** $\rho_M$ *versus* $\mathbf{N}$, calculated for the CN and mixed ($\theta = 0.25$) method, with different combinations of parameters

(values below $0.105$). The CN method with the relation $\tau = \min\{\rho c_p h^2/\kappa_{\max}, h\}$, on the other hand, results in Fig. 6, which reinforces the robustness of the method when we impose the stability criterion.

## 5 Final considerations

In this paper, we analyzed a family of finite difference schemes for a nonlinear heat equation, applied to a homogeneous silicon rod with Dirichlet boundary conditions. We show that the method is consistent with the conservative form of the nonlinear PDE, is conditionally TVD-stable and therefore converges to a weak solution. The focus is on implicit schemes, accelerated with an efficient Newton multigrid method, developed in composition with the Gauss-Seidel red-black smoother. Numerical experiments confirm the theory and show that the multigrid algorithm is robust to a range of values of the physical parameters, as well as being independent of the stability condition. The numerical tools used in this work can be extended to the two-dimensional case and are currently under development.

**Acknowledgements** The authors would like to acknowledge the Graduate Program in Numerical Methods for Engineering (PPGMNE) of the Federal University of Paraná (UFPR). The work of Adriano Rodrigues de Melo is supported by the Catarinense Federal Institute (IFC).

**Data availability** Data will be made available on request.

### Declarations

**Competing interests** The authors have no competing interests to declare that are relevant to the content of this article.

## References

1. Ibrahim, M., Olayiwola, R.O., Cole, A.T., Shehu, M.D., Muhammad, K.M.: Modeling and analytical simulation of high-temperature gas filtration combustion. J. Appl. Sci. Environ. Manage. **21**(5), 937–943 (2017). https://doi.org/10.4314/jasem.v21i5.20
2. Garikipati, K., Rao, V.S.: Recent advances in models for thermal oxidation of silicon. J. Comput. Phys. **174**(1), 138–170 (2001). https://doi.org/10.1006/jcph.2001.6884
3. Hristov, J.: An approximate analytical (integral-balance) solution to a nonlinear heat diffusion equation. Therm. Sci. **19**, 723–733 (2015). https://doi.org/10.2298/TSCI140326074H
4. Tucci, C., Trujillo, M., Berjano, E., Iasiello, M., Andreozzi, A., Vanoli, G.P.: Pennes' bioheat equation vs. porous media approach in computer modeling of radiofrequency tumor ablation. Sci. Rep. **11**(1), 5272 (2021). https://doi.org/10.1038/s41598-021-84546-6
5. Schaum, A., Koch, S., Kleindienst, M., Reichhartinger, M., Meurer, T., Moreno, J.A., Horn, M.: Observer design for a nonlinear heat equation: application to semiconductor wafer processing. J. Process Control. **119**, 34–43 (2022). https://doi.org/10.1016/j.jprocont.2022.09.004
6. Zhang, Y., Rabczuk, T., Lu, J., Lin, S., Lin, J.: Space-time backward substitution method for nonlinear transient heat conduction problems in functionally graded materials. Comput. Math. Appl. **124**, 98–110 (2022). https://doi.org/10.1016/j.camwa.2022.08.026
7. Filipov, S.M., Faragó, I.: Implicit Euler time discretization and FDM with Newton method in nonlinear heat transfer modeling. Int. Sci. J. "Math. Modeling" **2**(3), 94–98 (2018)

8. Filipov, S.M., Faragó, I., Avdzhieva, A.: Mathematical modelling of nonlinear heat conduction with relaxing boundary conditions. In: Georgiev, I., Datcheva, M., Georgiev, K., Nikolov, G. (eds.): Numerical methods and applications, pp. 146–158. Springer, Cham (2023)
9. Zen, P.D., Pinto, M.A.V., Franco, S.R.: A multigrid waveform relaxation method for solving the nonlinear silicon problem with relaxing boundary conditions. Numer. Heat Transf., Part B: Fundam. **86**(9), 3002–3017 (2025). https://doi.org/10.1080/10407790.2024.2351543
10. Maycock, P.D.: Thermal conductivity of silicon, germanium, III-V compounds and III-V alloys. Solid-State Electron. **10**(3), 161–168 (1967). https://doi.org/10.1016/0038-1101(67)90069-X
11. Lienemann, J., Yousefi, A., Korvink, J.G.: Nonlinear heat transfer modeling. In: Benner, P., Sorensen, D.C., Mehrmann, V. (eds.) Dimension reduction of large-scale systems, pp. 327–331. Springer, Berlin, Heidelberg (2005)
12. Rencz, M., Szekely, V.: Non-linearity issues in the dynamic compact model generation [package thermal modeling]. In: Ninteenth Annual IEEE Semiconductor Thermal Measurement and Management Symposium, pp. 263–270. (2003). https://doi.org/10.1109/STHERM.2003.1194372
13. Rencz, M., Szekely, V.: Studies on the nonlinearity effects in dynamic compact model generation of packages. IEEE Trans. Components Packag. Technol. **27**(1), 124–130 (2004). https://doi.org/10.1109/TCAPT.2004.825750
14. Rincon, M., Límaco, J., Liu, I.-S.: A nonlinear heat equation with temperaturedependent parameters. Math. Phys. Electron. J. ISSN 1086- 6655, **12**(3), 2006 (2006)
15. Hristov, J.: On a non-linear diffusion model of wood impregnation: analysis, approximate solutions, and experiments with relaxing boundary conditions. In: Singh, J., Anastassiou, G.A., Baleanu, D., Cattani, C., Kumar, D. (eds.) Advances in mathematical modelling, applied analysis and computation, pp. 25–53. Springer, Singapore (2023)
16. Krivovichev, G.V.: A computational approach to the modeling of the glaciation of sea offshore gas pipeline. Int. J. Heat Mass Transf. **115**, 1132–1148 (2017). https://doi.org/10.1016/j.ijheatmasstransfer.2017.08.117
17. Andreozzi, A., Brunese, L., Iasiello, M., Tucci, C., Vanoli, G.P.: Modeling heat transfer in tumors: a review of thermal therapies. Ann. Biomed. Eng. **47**(3), 676–693 (2019)
18. Kopp, P., Calo, V., Rank, E., Kollmannsberger, S.: Space-time hp-finite elements for heat evolution in laser powder bed fusion additive manufacturing. Eng. Comput. **38**(6), 4879–4893 (2022). https://doi.org/10.1007/s00366-022-01719-1
19. Nagel, L., Lippert, A., Tolle, T., Leonhardt, R., Zhang, H., Marić, T.: Stabilizing the unstructured volume-of-fluid method for capillary flows in microstructures using artificial viscosity. Exp. Comput. Multiphase Flow. **6**(2), 140–153 (2024). https://doi.org/10.1007/s42757-023-0181-y
20. Yee, H.C., Warming, R.F., Harten, A.: Implicit total variation diminishing (TVD) schemes for steady-state calculations. J. Comput. Phys. **57**(3), 327–360 (1985). https://doi.org/10.1016/0021-9991(85)90183-4
21. Mousa, M.M., Ma, W.-X.: Efficient modeling of shallow water equations using method of lines and artificial viscosity. Mod. Phys. Lett. B. **34**(4), 2050051 (2020). https://doi.org/10.1142/S0217984920500517
22. VonNeumann, J., RichtmyerR. D.: A method for the numerical calculation of hydrodynamic shocks. J. Appl. Phys. **21**(3), 232–237 (1950). https://doi.org/10.1063/1.1699639
23. Katayama, K., Hattori, M., Okada, M., Kotake, S.-I.: Numerical method of transient heat conduction with temperature dependent thermal properties. Bull. JSME. **15**(89), 1394–1401 (1972). https://doi.org/10.1299/jsme1958.15.1394
24. Jooma, R., Harley, C.: Heat transfer in a porous radial fin: analysis of numerically obtained solutions. Adv. Math. Phys. 2017(1)1658305 (2017). https://onlinelibrary.wiley.com/doi/pdf/10.1155/2017/1658305
25. Trottenberg, U., Oosterlee, C., Schüller, A.: Multigrid. Academic, San Diego (2001)
26. Malacarne, M.F., Pinto, M.A.V., Franco, S.R.: Performance of the multigrid method with time-stepping to solve 1D and 2D wave equations. Int. J. Comput. Methods Eng. Sci. Mech. **23**(1), 45–56 (2022). https://doi.org/10.1080/15502287.2021.1910750
27. Santiago, C.D., Ströher, G.R., Pinto, M.A.V., Franco, S.R.: A multigrid wave-form relaxation method for solving the Pennes bioheat equation. Numerical Heat Transfer, Part A: Applications **83**(9), 976–990 (2023) https://doi.org/10.1080/10407782.2022.2156411
28. Franco, S.R., Pinto, M.A.V.: A space-time multigrid method for poroelasticity equations with random hydraulic conductivity. Numer. Heat Transf., Part B: Fundam. **85**(9), 1226–1235 (2024). https://doi.org/10.1080/10407790.2023.2262746

29. Iserles, A.: A first course in the numerical analysis of differential equations, 1st edn. Cambridge University Press, Cambridge (1996)
30. LeVeque, R.J.: Numerical methods for conservation laws, 2nd edn. Birkhäuser, Berlin (1992)
31. Harten, A.: On a class of high resolution total-variation-stable finite-difference schemes. SIAM J. Numer. Anal. **21**(1), 1–23 (1984). https://doi.org/10.1137/0721001
32. Yee, H.C.: Construction of a class of symmetric TVD schemes. In: Dafermos, C., Ericksen, J.L., Kinderlehrer, D., Slemrod, M. (eds.) Oscillation theory, computation, and methods of compensated compactness, pp. 381–395. Springer, New York, NY (1986)
33. Oleinik, O.A., Kruzhkov, S.N.: Quasi-linear second-order parabolic equations with many independent variables. Russ. Math. Surv. **16**(5), 105–146 (1961). https://doi.org/10.1070/RM1961v016n05ABEH004114
34. Gavrilut, A., Morosanu, C.: Well-posedness for a nonlinear reaction-diffusion equation endowed with nonhomogeneous Cauchy-Neumann boundary conditions and degenerate mobility. ROMAI J. **14**(1), 129–141 (2018)
35. Oliveira, F., Franco, S.R., Pinto, M.A.V.: The effect of multigrid parameters in a 3D heat diffusion equation. Int. J. Appl. Mech. Eng. **23**(1), 213–221 (2018). https://doi.org/10.1515/ijame-2018-0012
36. Briggs, W.L., Henson, V.E., McCormick S.F.: A multigrid tutorial, 2nd edn. SIAM, Philadelphia (2000)
37. Wesseling, P.: An Introduction to multigrid methods. John Wiley & Sons, Chichester (1992)
38. Henson, V.E.: Multigrid methods nonlinear problems: an overview. In: Bouman, C.A., Stevenson, R.L. (eds.) Computational imaging, vol. 5016, pp. 36–48. SPIE. International Society for Optics and Photonics, Santa Clara, CA (2003). https://doi.org/10.1117/12.499473
39. Vandewalle, S.: Parallel multigrid waveform relaxation for parabolic problems. Teubner, Stuttgard (1993)
40. Incropera, F.P., Dewitt, D.P., Bergman, T.L., Lavine, T.L.: Fundamentals of heat and mass transfer, 6nd edn. John Wiley & Sons, NJ, USA (2006)
41. Silva, L.P., Rutyna, B.B., Righi, A.R.S., Pinto, M.A.V.: High order of accuracy for Poisson equation obtained by grouping of repeated Richardson extrapolation with fourth order schemes. Comput. Modeling Eng. Sci. **128**(2), 699–715 (2021). https://doi.org/10.32604/cmes.2021.014239
42. Oliveira, M.L., Pinto, M.A.V., Rodrigo, C., Gaspar, F.J.: Modified Picard with multigrid method for two-phase flow problems in rigid porous media. Int. J. Numer. Methods Eng. **125**(5), 7397 (2024). https://doi.org/10.1002/nme.7397